Proceedings of the Sixth IASTED International Conference
BIOMEDICAL ENGINEERING
February 13–15, 2008, Innsbruck, Austria
ISBN Hardcopy: 978-0-88986-721-5 / CD: 978-0-88986-722-2

INTEGRATION OF THE CIRCLE OF WILLIS INTO AVOLIO'S MODEL OF THE ARTERIAL HAEMODYNAMICS

Michael Schwarz, Minh P. Nguyen, Uwe Kiencke
Institute of Industrial Information Technology
Universität Karlsruhe (TH)
Karlsruhe, Germany
email: schwarz@iiit.uni-karlsruhe.de

Claudia Heilmann, Rolf Klemm,
Christoph Benk, Friedhelm Beyersdorf
Department of Cardiovascular Surgery
University Medical Center Freiburg
Freiburg, Germany

Hans-Jörg Busch
Department of Cardiology and Angiology
University Medical Center Freiburg
Freiburg, Germany

ABSTRACT
Operations on the open heart require perfusion of the body by a heart-lung machine. A sufficient perfusion of vital organs is essential and has to be guaranteed also for patients with severe stenoses of the carotid arteries. Models of the arterial system offer the opportunity to simulate arterial flow and pressure in organs that cannot be accessed by direct measurement. They can support surgical planning and provide real-time information during the operation itself. In 1980 A. P. Avolio published a 1D model of the arterial haemodynamics. It consists of a branching system of 128 arterial segments which represent short elastic tubes. Avolio's model assumes a tree-like structure of the arterial system. However this is not appropriate for the brain: The anterior and posterior communicating arteries are missing in this approach. The Circle of Willis becomes important in case of an asymmetric perfusion of the brain. In this paper we show how this redundant structure can be integrated into Avolio's model using a state-space representation. Simulation results demonstrate significant differences between Avolio's model and our model if a carotid artery is stenosed.

KEY WORDS
Haemodynamics, cerebral perfusion, Circle of Willis, transmission line model

1. Introduction

Distributed models of the arterial haemodynamics have been a subject of research since the 1960s (overviews are given by Westerhof and Stergiopulos [18] and John [11]). Models considering the whole arterial system are mostly implemented as 1D models, which assume a monophase, laminar flow. A popular approach are so-called transmission line models which are described in section 2. This section shows how state-space equations can be obtained from the original transmission line equation.

Avolio's model [2] is an established transmission line model which approximates the topology of the arterial system with 128 segments. It is suitable to simulate pulsatile blood flow and pressure in the systemic arteries and has therefore been used as a basis for model based monitoring of patients undergoing cardiac surgery by Naujokat and Kiencke [15].

However with its tree-like structure Avolio's model fails to predict cerebral blood flow in case of an asymmetric perfusion of the brain. The anterior and posterior communicating arteries, which prevent insufficient perfusion, are missing in Avolio's topology. Asymmetric perfusion occurs when a carotid artery is stenosed or when antegrade cerebral perfusion is applied during Deep Hypothermic Circulatory Arrest. Therefore the integration of the Circle of Willis into Avolio's model, shown in section 3 is crucial to simulate cerebral haemodynamics.

The results for asymmetric perfusion of Avolio's model and the enhanced model are compared in section 4.

2. Transmission line models

2.1 Electrical analogon of haemodynamics

Arteries can be modelled as cylindric elastic tubes. Simplifying assumptions, e. g. monophase, laminar flow, rotational symmetry, negligence of the effect of gravitation and consideration of blood as a homogeneous fluid lead to a linearized one-dimensional form of the Navier-Stokes equations [11, 12]:

$$-\frac{\partial p}{\partial z} = \frac{\rho}{\pi r^2} \cdot \frac{\partial q}{\partial t} + \frac{8\eta}{\pi r^4} \cdot q \tag{1a}$$

$$-\frac{\partial q}{\partial z} = \frac{3\pi r^3}{2Ed} \cdot \frac{\partial p}{\partial t} \tag{1b}$$

where $p =$ pressure, $q =$ flow, $\rho =$ density of blood, $\eta =$ dynamic viscosity of blood, $r =$ radius of the vessel, $d =$ arterial wall thickness and $E =$ Young's modulus.

Figure 1 shows a section of an electrical transmission line. It represents equation (1) if pressure is replaced by voltage and blood flow by electric current and if the fol-

lowing coefficients are introduced:

$$R' = \frac{dR}{dz} = \frac{8\eta}{\pi r^4} \quad \text{resistance per unit length}$$
$$L' = \frac{dL}{dz} = \frac{\rho}{\pi r^2} \quad \text{inductance per unit length}$$
$$C' = \frac{dC}{dz} = \frac{3\pi r^3}{2Ed} \quad \text{capacitance per unit length}$$

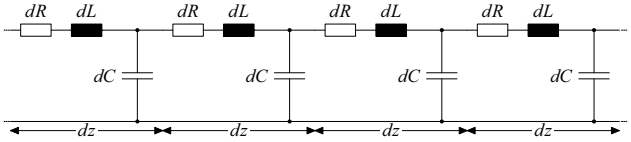

Figure 1. Electrical transmission line

The coherence between the input and output pressure and flow is given by the following equation for a harmonic stimulus and a steady-state system [9, 11]:

$$p_{in} = p_{out} \cosh \gamma \Delta z + q_{out} Z_0 \sinh \gamma \Delta z$$
$$q_{in} = p_{out} Z_0^{-1} \sinh \gamma \Delta z + q_{out} \cosh \gamma \Delta z$$

where $\Delta z =$ length of transmission line,

$$Z_0 = \sqrt{(R' + j\omega L')/j\omega C'} \quad \text{characteristic impedance,}$$
$$\gamma = \sqrt{(R' + j\omega L') \cdot j\omega C'} \quad \text{propagation constant.}$$

Arbitrary periodic stimuli can be simulated applying Fourier series expansion.

2.2 Discretization

Another approach to solve the partial differential equation (1) is used in our model. Ordinary differential equations are obtained discretizing the flow direction z and ODE solvers can be applied for simulation. Thus, transient behaviour can be simulated and a modular implementation in a simulation tool is possible. The approximation is appropriate for short arterial segments. Figure 2 shows valid discretizations of a transmission line of the length Δz with $R = R'\Delta z$, $L = L'\Delta z$, $C = C'\Delta z$. We call a discretization *valid*, if the PDE (1) is the limit of the ODE for $\Delta z \to dz$.

The following steps can be carried out to proof validity:

1. Set up the (Laplace) chain matrix $\underline{A}$ for the quadripole (cf. [8]):

$$\begin{bmatrix} p_{in} \\ q_{in} \end{bmatrix} = \underline{A} \cdot \begin{bmatrix} p_{out} \\ q_{out} \end{bmatrix} = \begin{bmatrix} A & B \\ C & D \end{bmatrix} \cdot \begin{bmatrix} p_{out} \\ q_{out} \end{bmatrix}$$

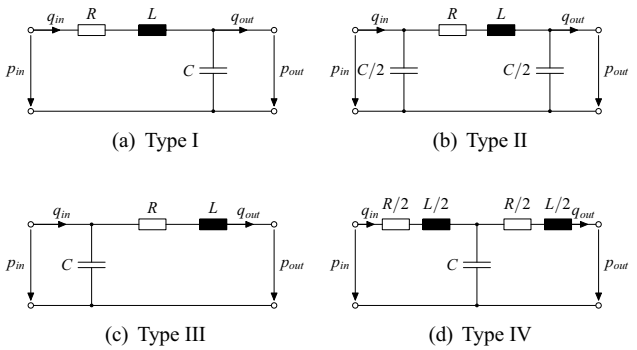

(a) Type I (b) Type II

(c) Type III (d) Type IV

Figure 2. Discrete quadripoles

2. With the $ABCD$-parameters

$$D \cdot p_{in} - \det \underline{A} \cdot p_{out} = B \cdot q_{in}$$
$$q_{in} - D \cdot q_{out} = C \cdot p_{out}$$

holds.

3. Calculate the inverse Laplace transform and the limit $\Delta z \to dz$.

There is also an illustrative explanation for the equivalence of the four quadripoles for very short vessels: For $\Delta z \to dz$ the pressure difference across the resistor and the inductor as well as the flow through the capacitor converge to zero. Therefore, the position of the capacitor is not relevant.

Various situations occur in terms of boundary conditions for the quadripoles when modelling complex networks of vessels. The different types of segments allow a state-space representation for these situations.

Type I: Known input pressure and output flow.

$$\frac{dp_{out}}{dt} = \frac{1}{C} \cdot (q_{in} - q_{out})$$
$$\frac{dq_{in}}{dt} = -\frac{R}{L} \cdot q_{in} + \frac{1}{L} \cdot (p_{in} - p_{out})$$

This situation occurs when modelling branching vessels: Let segments 2 and 3 be the successors of segment 1. Then $p_{in}^2 = p_{in}^3 = p_{out}^1$ and $q_{out}^1 = q_{in}^2 + q_{in}^3$ holds. Thus pressure information is passed to the succeeding segments and flow information is propagated backwards.

Type II: Known input and output flow.

$$\frac{dp_{in}}{dt} = \frac{2}{C} \cdot (q_{in} - q_{RL})$$
$$\frac{dp_{out}}{dt} = \frac{2}{C} \cdot (q_{RL} - q_{out})$$
$$\frac{dq_{RL}}{dt} = -\frac{R}{L} \cdot q_{RL} + \frac{1}{L} \cdot (p_{in} - p_{out})$$

where q_{RL} = flow through R and L. Type II can be used as an initial segment of the arterial system with a flow source as a heart model connected left hand side and a type I segment connected right hand side. This situation concerning the boundary conditions also occurs at the posterior communicating arteries (cf. section 3).

Type III: Known input flow and output pressure.

$$\frac{dp_{in}}{dt} = \frac{1}{C} \cdot (q_{in} - q_{out})$$
$$\frac{dq_{out}}{dt} = -\frac{R}{L} \cdot q_{out} + \frac{1}{L} \cdot (p_{in} - p_{out})$$

This segment type is suitable for anastomosing structures, e. g. to model the venous system.

Type IV: Known input and output pressure.

$$\frac{dp_C}{dt} = \frac{1}{C} \cdot (q_{in} - q_{out})$$
$$\frac{dq_{in}}{dt} = -\frac{R}{L} \cdot q_{in} + \frac{2}{L} \cdot (p_{in} - p_C)$$
$$\frac{dq_{out}}{dt} = -\frac{R}{L} \cdot q_{out} + \frac{2}{L} \cdot (p_C - p_{out})$$

where p_C = pressure difference across the capacitor C. This situation occurs at the anterior communicating artery (cf. section 3).

2.3 Peripheral blood flow

Arterioles and capillaries provide the greatest portion of the total vascular resistance. However, their inductance and capacitance is negligible because of their small diameters. Therefore only larger vessels are modelled as quadripoles whereas smaller vessels are concentrated in variable *terminal resistors*. If venous pressure is neglected, the terminal resistors are grounded.

The terminal resistors determinate the total vascular resistance (and thus arterial pressure) as well as the distribution of blood flow in the body. In many applications physiological flow rates and pressure values are used to determine an initial configuration of the terminal resistors (cf. [11]). Flow rates for the brain are given e. g. by Fahrig et al. [5]. Variable resistors allow to implement vasomotor control mechanisms like the baroreceptor mechanism or autoregulation of vital organs. Models of control mechanisms are discussed by Guyton et al. [7]. Naujokat and Kiencke [15] introduce an online adaptation method of the total vascular resistance for real-time simulation.

2.4 Avolio's model

An established transmission line model of the human arterial system was presented by Avolio [2]. The topology of the model is shown in figure 3. The graph has got a tree-structure and consists of 128 segments. The nomenclature of the segments and anatomical data is given in [2].

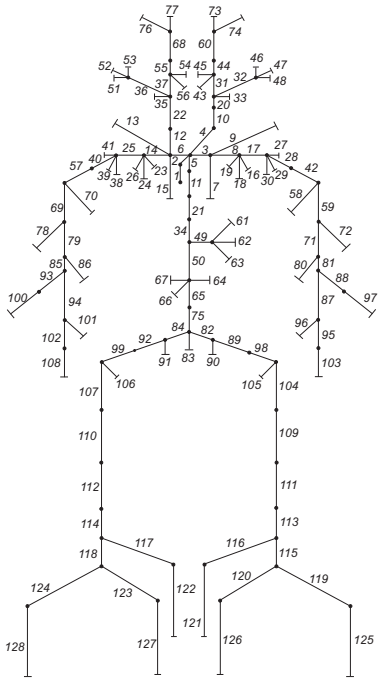

Figure 3. Topology of Avolio's model

Segment 1 (ascending aorta) is the initial segment of the model. The output flow of the left ventricle has to be given to run a simulation. The initial segment is modelled as a type II quadripole which requires a flow signal as a boundary condition at its input and output. The input flow is the cardiac output, the output flow information is propagated backwards from segment 2 (aortic arch) which is a type I quadripole. The initial segment generates a pressure information at its input and the output. The input pressure is identical to the systemic arterial pressure, the output pressure is passed to segment 2 as a boundary condition. All subsequent quadripoles are of type I. Pressure information is passed to the successors while flow information is returned to the predecessors as described in section 2.2.

A state space model of the order 257 is obtained with one type III quadripole and 127 type I quadripoles, including 61 terminal resistors. Thus, the model causes high computational effort but it is suitable to simulate pulsatile pressure and flow curves.

Simpler topologies may be sufficient depending on the application. Such approaches are discussed e. g. by Stergiopulos et al. [17] and Misgeld and Hexamer [13]. However, supervision of cerebral perfusion even requires to increase complexity of the topology of the brain.

3. Integration of the Circle of Willis

The brain is sensitive to insufficient perfusion and may suffer irreversible damage from ischemia. Stenoses or occlusions of afferent arteries (carotid and vertebral arteries) can be compensated by vasomotor control and a redundant ar-

terial system in the brain. In Avolio's model the vertebral arteries are modelled as terminal segments. Thus a tree structure is maintained. However, the vertebral arteries actually anastomose into the basilar artery which bifurcates to the posterior cerebral arteries. Furthermore, the posterior and middle cerebral arteries are connected by the posterior communicating arteries while the anterior communicating artery links the right and left anterior cerebral artery. The entire topology is shown in figure 4.[1] The physiological data (table 1) is taken from Avolio [2] and Alastruey et al. [1]. The radius of the postcommunicating arteries suggested by Alastruey et al. [1] leads to an overestimation of the flow in these arteries. Therefore a smaller radius has been chosen for the communicating arteries (cf. [4, 5, 10]).

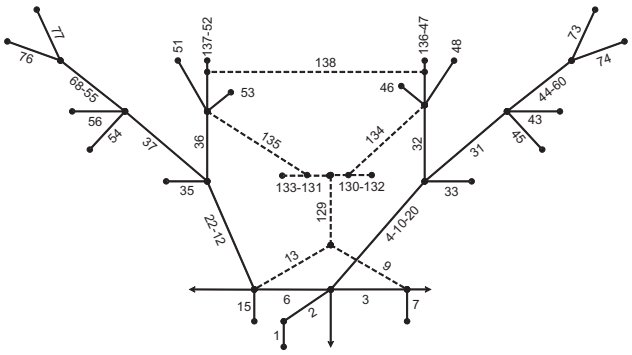

Figure 4. Topology of the head including the Circle of Willis

The Circle of Willis (CoW) is modelled with the segments introduced in section 2.2. The adjacent vessels (modelled with type I segments) which are part of Avolio's model determine the boundary conditions. An "input port" of the CoW is connected to the output port of a type I segment which means that the input pressure is given by Avolio's model at this point. In figure 5, the segments 3 (left subclavian), 6 (brachiocephalic), 32 and 36 (left and right internal carotid) are connected to input ports. An "output port" is connected to the input port of a type I segment, thus the output flow is given by Avolio's model. The segments 132, 133 (left and right posterior cerebral artery, postcommunicating part), 47 and 52 (left and right anterior cerebral artery, postcommunicating part) are connected to output ports. The CoW system must deliver an input flow for each input port and an output pressure for each output port. The boundary conditions determine the types of segments that have to be chosen.

The state-space representation of the CoW system can be derived from the state-space equations of the segments and the flow balances and pressure conditions at the vertices, where the quadripoles are connected. The approach is illustrated for the vertebral arteries in the sequel.

The vertebral arteries are modelled by type I segments. The input pressure of the left vertebral artery is determined by the output pressure of the left subclavian artery $p_{in}^{9} = p_{out}^{3}$ and the input pressure of the right vertebral artery is equal to the output pressure of the brachiocephalic artery $p_{in}^{13} = p_{out}^{6}$. The two vertebral arteries anastomose to the basilar artery, therefore $p_{in}^{129} = p_{out}^{9} = p_{out}^{13}$ holds. Thus, the following equations result:

[1] The branches of the internal and external carotid arteries have been swapped to increase clarity of the diagram.

Table 1. Physiological data

Segment	left	right	Δz cm	r cm	d cm	E 10^6 Pa
Data from Avolio [2]						
Ascending aorta	1		4	1.45	0.163	0.4
Aortic arch	2		2	1.12	0.132	0.4
Aortic arch	5		3.9	1.07	0.127	0.4
Subclavian A	3		3.4	0.42	0.067	0.4
Subclavian B	8	14	6.8	0.4	0.066	0.4
Common carotid A	4	12	8.9	0.37	0.063	0.4
Common carotid B	10	22	8.9	0.37	0.063	0.4
Common carotid C	20		3.1	0.37	0.63	0.4
Brachiocephalic	6		3.4	0.62	0.086	0.4
Internal mammary	7	15	15	0.1	0.03	0.8
Vertebral	9	13	14.8	0.19	0.045	0.8
External carotid A	31	37	5.9	0.18	0.045	0.8
External carotid B	44	55	5.9	0.13	0.039	0.8
External carotid C	60	68	5.9	0.08	0.026	1.6
Internal carotid	32	36	11.8	0.15	0.042	0.8
Superior thyroid l	33	35	4	0.07	0.02	0.8
Lingual	43	56	3	0.1	0.03	0.8
Facial	45	54	4	0.1	0.03	1.6
Middle cerebral	46	53	3	0.06	0.02	1.6
Anterior cerebral B	47	52	5.9	0.08	0.026	1.6
Ophthalmic	48	51	3	0.07	0.02	1.6
Superficial temporal	73	77	4	0.06	0.02	1.6
Maxiliary	74	76	5	0.07	0.02	1.6
Data from Alastruey et al. [1]						
Basilar	129		2.9	0.162	0.04	1.6
Posterior cerebral A	130	131	0.5	0.107	0.027	1.6
Posterior cerebral B	132	133	8.6	0.105	0.026	1.6
Posterior comm.	134	135	1.5	0.05*	0.018	1.6
Anterior cerebral A	136	137	1.2	0.117	0.029	1.6
Anterior comm.	138		0.3	0.05*	0.019	1.6

* adapted to Fahrig et al. [5]

Left vertebral artery:

$$\frac{dp_{in}^{129}}{dt} = \frac{1}{C^9} \cdot (q_{in}^9 - q_{out}^9) \tag{2}$$

$$\frac{dq_{in}^9}{dt} = -\frac{R^9}{L^9} \cdot q_{in}^9 + \frac{1}{L^9} \cdot (p_{out}^3 - p_{in}^{129}) \tag{3}$$

Right vertebral artery:

$$\frac{dp_{in}^{129}}{dt} = \frac{1}{C^{13}} \cdot (q_{in}^{13} - q_{out}^{13}) \tag{4}$$

$$\frac{dq_{in}^{13}}{dt} = -\frac{R^{13}}{L^{13}} \cdot q_{in}^{13} + \frac{1}{L^{13}} \cdot (p_{out}^6 - p_{in}^{129}) \tag{5}$$

We calculate $C^9 \cdot (2) + C^{13} \cdot (4)$

$$(C_9 + C_{13}) \frac{dp_{in}^{129}}{dt} = q_{in}^9 - q_{out}^9 + q_{in}^{13} - q_{out}^{13}$$

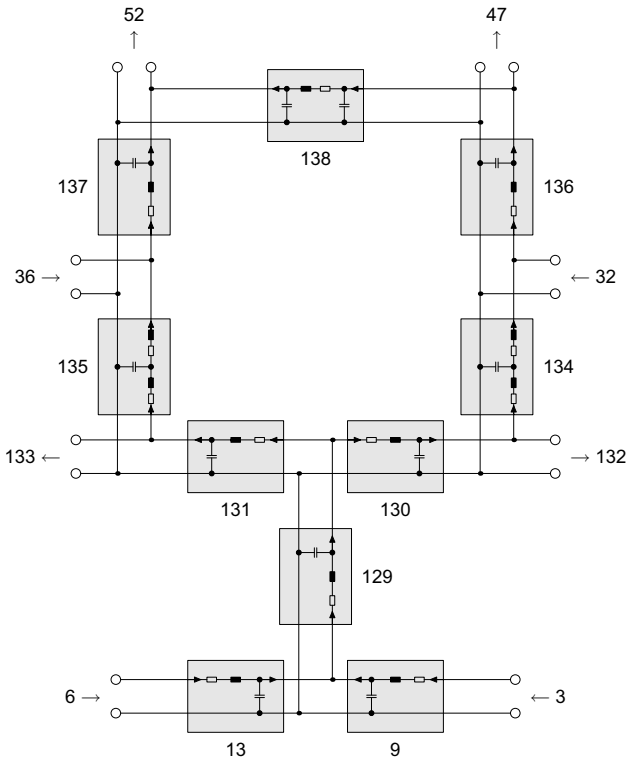

Figure 5. Model of the Circle of Willis with interface to Avolio's model

and insert the flow balance $q_{in}^{129} = q_{out}^{9} + q_{out}^{13}$:

$$\frac{dp_{in}^{129}}{dt} = \frac{1}{C^9 + C^{13}} \cdot (q_{in}^{9} + q_{in}^{13} - q_{in}^{129}) \qquad (6)$$

Equations (2), (4) and (6) are state-space equations of the system. Twenty equations are required to describe the complete CoW system.

4. Results and Discussion

A simulation of the system has been carried out with a heart rate of $60\,\mathrm{min}^{-1}$ and a cardiac output of $85\,\mathrm{ml/s}$. The course of the aortic flow is taken from [16]. The obtained average flows in the cerebral and communicating arteries (see table 2, left) as well as the vertebral and internal carotid arteries approximately match with the simulation results of Fahrig's cerebrovascular flow phantom [5]. The parametrization of the terminal resistors (cf. section 2.3) is a compromise between a realistic total cerebral blood flow entering through the internal carotid and vertebral arteries and a realistic flow leaving the anterior, middle and posterior cerebral artery. The discrepancy arises because smaller vessels like the superior cerebellar artery are neglected by the model [5].

An area stenosis of 90 % in the right internal carotid artery (segment 36) has been simulated varying the characteristics of the quadripole to contrast the results of Avolio's model and the new model including the Circle of Willis. Figure 6(a) shows that Avolio's model predicts a significantly reduced flow in the right anterior cerebral artery. However, the new model (figure 6(b)) shows that the collateral blood flow through the anterior and posterior communicating (figure 8) arteries compensates the reduced flow through the right internal carotid artery, while flow through the left anterior cerebral artery is slightly diminished. Similar results are obtained for the middle cerebral artery (figure 7).[2]

The average flows in the cerebral and communicating arteries are given in table 2, right. Obviously, the compensation of the reduced perfusion of the right brain is mainly due to the collateral flow through the anterior communicating artery, which has also been observed by Alastruey [1].

Table 2. Simulated average flow in $\mathrm{ml/s}$

	physiological		ICA stenosis	
Segment	left	right	left	right
Anterior cerebral	1.37	1.37	1.36	1.28
Mean cerebral	2.50	2.50	2.51	2.32
Posterior cerebral	0.93	0.93	0.95	0.95
Anterior communicating	-0.01		2.67	
Posterior communicating	0.31	0.31	0.50	0.42

5. Conclusion and Outlook

Avolio's model of the arterial haemodynamics has been extended by the Circle of Willis in this article. Electrical quadripoles are used to map the transmission line equations to a linear state-space model. The complete Circle of Willis is modelled as a system of coupled quadripoles with a defined interface to Avolio's model. The resulting model can be simulated using ODE solvers.

The model is designed to simulate perfusion of vital organs. Simulation results are consistent with the results of other authors. Significant differences between Avolio's model and the extended model occur in case of an asymmetric perfusion of the brain. The extended model is capable to predict more realistic flow rates in the brain for patients with stenoses of the carotid arteries.

Up to now we assume a complete Circle of Willis in our model. Anatomical variations like absent arteries [1, 6] or variations in the diameter [3] may be diagnosed in surgical planning and considered in future versions of the model. Moreover, vasomotor control [6, 14] is not yet considered, however the model structure allows to implement changes in peripheral resistance. Autoregulation might contribute to compensate the effects of asymmetric perfusion. In a modified version the model will be capable to predict cerebral flow during antegrade cerebral perfusion.

[2] The pulsatile dynamics of the anterior and middle cerebral artery are almost identical because they branch from the same vertex. However their amplitudes differ.

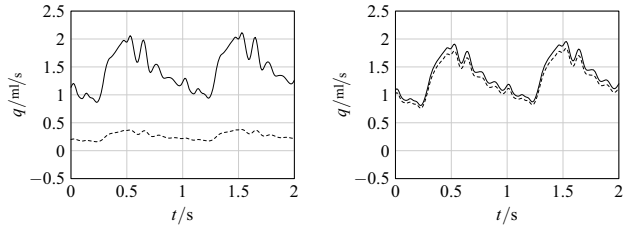

(a) Avolio's model (b) Model with Circle of Willis

Figure 6. Flow in anterior cerebral arteries (– left, - - right)

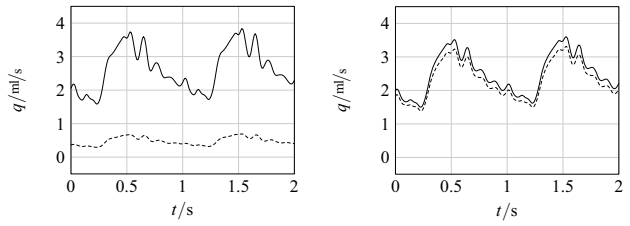

(a) Avolio's model (b) Model with Circle of Willis

Figure 7. Flow in middle cerebral arteries (– left, - - right)

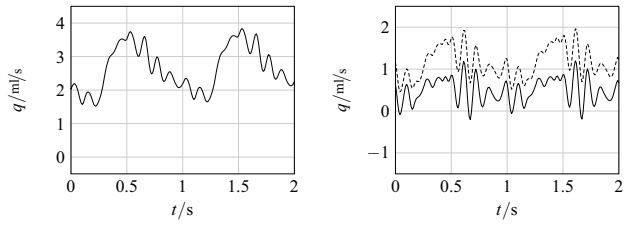

(a) Flow in anterior communicating artery (b) Flow in posterior communicating arteries (– left, - - right)

Figure 8. Model with Circle of Willis

References

[1] J. Alastruey, K. H. Parker, J. Peiró, S. M. Byrd, and Sherwin, S. J., Modelling the circle of Willis to assess the effects of anatomical variations and occlusions on cerebral flows, *J Biomech*, 40(8), 2007, 1794–805.

[2] A. P. Avolio, Multi-branched model of the human arterial system, *Med Biol Eng Comput*, 18, 1980, 709–718.

[3] F. Cassot, V. Vergeur, P. Bossuet, B. Hillen, M. Zagzoule, and J. P. Marc-Vergnes, Effects of anterior communicating artery diameter on cerebral hemodynamics in internal carotid artery disease. A model study, *Circulation*, 92(10), Nov 1995, 3122–31.

[4] K. Cieślicki and D. Cieśla, Investigations of flow and pressure distributions in physical model of the circle of Willis, *J Biomech*, 38(11), Nov 2005, 2302–10.

[5] R. Fahrig, H. Nikolov, A. J. Fox, and D. W. Holdsworth, A three-dimensional cerebrovascular flow phantom, *Med Phys*, 26(8), Aug 1999, 1589–99.

[6] A. Ferrández, T. David, and M. D. Brown, Numerical models of auto-regulation and blood flow in the cerebral circulation, *Comput Methods Biomech Biomed Engin*, 5(1), Feb 2002, 7–19.

[7] A. C. Guyton, T. G. Coleman, and Harris H. J., Circulation: Overall Regulation, *Annual Review of Physiology*, 34, 1972, 13–46.

[8] M. A. Helal, Derivation of closed-form expression for the cerebral circulation models, *Comput Biol Med*, 24(2), Mar 1994, 103–18.

[9] M. A. Helal, K. C. Watts, A. E. Marble, and S. N. Sarwal, Theoretical model for assessing haemodynamics in arterial networks which include bypass grafts, *Med Biol Eng Comput*, 28(5), Sep 1990, 465–73.

[10] B. Hillen, B. A. Drinkenburg, H. W. Hoogstraten, and L. Post, Analysis of flow and vascular resistance in a model of the circle of Willis, *J Biomech*, 21(10), 1988, 807–14.

[11] L. R. John, Forward electrical transmission line model of the human arterial system, *Med Biol Eng Comput*, 42(3), May 2004, 312–21.

[12] J. R. LaCourse, G. Mohanakrishnan, and K. Sivaprasad, Simulations of arterial pressure pulses using a transmission line model, *J Biomech*, 19(9), 1986, 771–80.

[13] B. J. E. Misgeld and M. Hexamer, Modellierung und Regelung des arteriellen Blutflusses während der extrakorporalen Zirkulation, *at*, 9, 2005, 454–461.

[14] K. T. Moorhead, J. G. Chase, T. David, and J. Arnold, Metabolic model of autoregulation in the Circle of Willis, *J Biomech Eng*, 128(3), Jun 2006, 462–6.

[15] E. Naujokat and U. Kiencke, Beobachtung des Patientenzustands bei Herzoperationen, *at*, 50(5), 2002, 204–211.

[16] M. F. O'Rourke, R. P. Kelly, and A. P. Avolio, *The arterial pulse* (Lea & Febiger, 1992).

[17] N. Stergiopulos, D. F. Young, and T. R. Rogge, Computer simulation of arterial flow with applications to arterial and aortic stenoses, *J Biomech*, 25(12), Dec 1992, 1477–88.

[18] N. Westerhof and N. Stergiopulos, Models of the arterial tree, *Stud Health Technol Inform*, 71, 2000, 65–77.